Polymer Chemistry

ROYAL SOCIETY OF CHEMISTRY

PAPER

View Article Online
View Journal | View Issue

Cite this: *Polym. Chem.*, 2023, **14**, 848

Pre- and post-functionalization of thermoresponsive cationic microgels with ionic liquid moieties carrying different counterions†

Thomke Belthle, [a,b] Marcus Lantzius-Beninga [b] and Andrij Pich *[a,b,c]

Herein, we study the incorporation of hydrophilic-to-amphiphilic alkylated *N*-vinylimidazolium based ionic liquid monomers with different counter anions into *N*-vinylcaprolactam (VCL) based microgels *via* precipitation polymerization, and their resulting properties. Two strategies, following either a pre-functionalization of the comonomers by counterion exchange with subsequent polymerization, or post-functionalization *via* counterion exchange on pre-synthesized microgels, are applied and compared. The employed anions, *i.e.*, halides (X^-), methanesulfonate (MeS^-), tetrafluoroborate (BF_4^-), and bistriflimide (NTf_2^-), were selected because of their kosmotropic-to-chaotropic solution properties. The resulting microgels with 10 mol% degree of functionalization were characterized by light scattering techniques, particularly with respect to their temperature-dependent swelling behavior and electrophoretic mobility. Differences in the counterion effect can be correlated to the solvation of the anions given by the Hofmeister series, cation–anion interaction strength, as well as the hydrophobicity of the vinylimidazolium moiety, *i.e.*, the alkyl chain length. In this context, chaotropic anions will lead to a decrease in microgel size and electrophoretic mobility, while the volume phase transition temperature decreases as a function of the alkyl chain length. Moreover, the pre-functionalization approach can give access to different morphologies, such as anisotropic microgels, while generally restricting the microgel swelling, compared to the post-functionalization approach. Our results will allow for the controlled design of new functional microgels *via* simple precipitation polymerization with potential applications in drug delivery, biocatalysis and self-healing materials.

Received 24th November 2022,
Accepted 19th January 2023

DOI: 10.1039/d2py01477g

rsc.li/polymers

Introduction

Microgels are an interesting class of cross-linked polymer colloids exhibiting a porous structure, ability to swell in water and organic solvents and adaptive mechanical properties.[1,2] They can form stable dispersions in water and show responsiveness to external stimuli such as pH, ionic strength,[3] light,[4] and temperature. Microgels based on *N*-vinylcaprolactam (VCL) have gained interest in the field of smart polymer materials for biological and medical applications, due to their biocompatibility and tunable temperature-responsive behavior. Upon heating, PVCL-based microgels show a decrease in swelling and volume due to the collapse of the polymer chains confined in the network, which is induced by disruption of hydrogen bonds and poor solvation by water molecules. The incorporation of charges, either pH dependent[5,6] or independent,[7] provides the possibility of enhanced stability in solution, as well as the ability for electrostatic interactions between the microgels and payload.[8] Additionally, the thermoresponsive behavior of microgels is strongly affected by the incorporation of ionizable groups, which can lead to a shift of the volume phase transition temperature (VPTT), *i.e.*, the point of inflection of the temperature-dependent hydrodynamic diameter.[5] Another interesting application of microgels is their ability to act as carriers for active molecules, which are otherwise not soluble or stable in aqueous solution.[9] Systems for the stabilization of hydrophobic drugs such as doxorubicin,[10] ibuprofen,[9,11] and diclofenac[12] have been intensively studied proving the demand for colloidal carriers that enable the transport of lipophilic substances in an aqueous environment. In this context, the controlled manipulation of the internal microgel structure can be the key to high loading efficiency at preserved colloidal stability.[13] Moreover, the introduction of functional amphiphilic-to-hydrophobic comonomers can sig-

[a]*DWI - Leibniz-Institute for Interactive Materials, Forckenbeckstraße 50, 52074 Aachen, Germany. E-mail: pich@dwi.rwth-aachen.de*
[b]*Functional and Interactive Polymers, Institute of Technical and Macromolecular Chemistry, RWTH Aachen University, Worringerweg 2, 52074 Aachen, Germany*
[c]*Aachen Maastricht Institute for Biobased Materials (AMIBM), Maastricht University, Brightlands Chemelot Campus, Urmonderbaan 22, 6167 RD Geleen, The Netherlands*

† Electronic supplementary information (ESI) available. See DOI: https://doi.org/10.1039/d2py01477g

nificantly alter the solution behavior of temperature-responsive microgels,[14] as well as their morphology.[15,16]

Ionic liquids are an attractive class of new solvents that combine the properties and structural characteristics of salts, with the low melting temperature of organic solvents. A variety of different, suitable anions and cations is described in the literature, which in principle lead to the formation of ionic liquids in any combination.[17] Depending on the nature of these ions, which can be either inorganic or organic, completely different chemical and physical properties can be introduced. Some of the available cations can be further functionalized with polymerizable groups, which enable the formation of poly(ionic liquids). Poly(ionic liquids) are characterized by the crystallinity and high conductivity of ionic liquids but can additionally show thermoresponsive behavior, and swelling ability in different solvents.[18] This behavior is strongly influenced by the cation–anion interactions. Karjalainen *et al.* reported the change from LCST-like to UCST-like behavior for polycations such as poly(2-(dimethylamino)ethyl methacrylate), (PDMAEMA), by using $[NTf_2]^-$ anion salt.[19,20] In another publication from Jana *et al.* a coexistence of LCST and UCST was reported for linear random poly(ionic liquid) copolymers based on poly[oligo(2-ethyl-2-oxazoline)acrylate].[21] One of the investigated comonomers was 1-vinyl-3-butylimidazolium bromide, which, polymerized as homopolymer, only shows UCST-like behavior in the presence of halide ions. Thus, vinylimidazolium derived comonomers are interesting to potentially introduce a UCST-like solution behavior in LCST-like behaving polymer materials. Poly(ionic liquid) colloidal beads have been synthesized using an ionic liquid monomer and a cross-linking agent in a microfluidic device by Rahman *et al.*[22] The authors studied the swelling ability of these hydrogel beads by anion exchange with various counterions. Poly(ionic liquid) nanogels possessing a UCST-type solution behavior were produced by Chen *et al.* using a post-functionalization approach for the latter application in catalysis.[23] In addition, smart gels with incorporated poly(ionic liquid) moieties are interesting materials for application in the electrochemical field, smart sensors,[24] as well as for the immobilization of peptides or enzymes,[25] or as antimicrobial wound dressing.[26,27] Very little attention has been payed so far to the effect of the counterion nature on characteristic properties, such as the stimuli-responsiveness in microgels with incorporated poly(ionic liquid) compartments.

In this work, we present and compare two different ways for the formation of cationic microgels with poly(ionic liquid) moieties, and characterization of the effect of the counterion nature on the microgel properties. Owing to the ionic liquid properties of vinylimidazolium salts, a polymerizable form of this cation was chosen as the functional comonomer. Microgels based on *N*-vinylcaprolactam (VCL) and cationic moieties from 1-vinyl-3-methylimidazolium iodide ($VIM^+C_1H_3[I]^-$),[7] and 1-vinyl-3-alkylimidazolium bromide ($VIM^+C_nH_{2n+1}[Br]^-$, n = 12–16) have been synthesized before, and show interesting property changes depending on the alkyl chain length attached to the charge.[28] Thus, these systems serve as reference for the analysis of microgels with more complex counter anions. The two approaches for the formation of poly(VCL-*co*-$VIM^+C_nH_{2n+1}[A]^-$) microgels (with variation of n, and $[A]^-$) can be described as the pre-functionalization of the monomer *via* anion exchange with subsequent polymerization for the formation of microgels (Scheme 1a), and post-functionalization of pre-synthesized microgels by anion exchange on microgel dispersions (Scheme 1b). In both scenarios, the microgel synthesis is performed by simple precipitation polymerization without additional surfactants. Anions applied in the formation of microgels are varied from halide ($[X]^-$ = $[Br]^-$, $[I]^-$) to hydrophilic organic (methanesulfonate; $[MeS]^-$), inorganic (tetrafluoroborate; $[BF_4]^-$), and hydrophobic organic (bistriflimide; $[NTf_2]^-$) in nature. These anions can be compared regarding their hydrogen bond accepting character. Precisely, $[Br]^-$ is a better hydrogen bond acceptor, which is leading to stronger interionic interactions and a higher lattice energy than, *e.g.*, bistriflimide. An order according to the strength of the H-bonds is given by the Hofmeister series and can be established as follows:[29]

$$[Br]^- > [I]^- > [MeS]^- > [BF_4]^- > [NTf_2]^-.$$

Moreover, the counterions can be distinguished with regard to kosmotropic-to-chaotropic properties. While kosmotropes enable hydrogen bonds and can thereby increase, *e.g.*, protein stability in solution (salting-out), chaotropes impede ordered hydrogen bonds (salting-in). Therefore, we hypothesize that the nature of the present anion will influence the solution behavior of poly(VCL-*co*-$VIM^+C_nH_{2n+1}[A]^-$) microgels.

Experimental section

Materials

N-Vinylcaprolactam (VCL) (Sigma-Aldrich, 98%) was distilled and recrystallized from *n*-hexane before use. The quaternized monomer was synthesized from *N*-vinylimidazole (Sigma Aldrich, 99%) after removal of the inhibitor using basic Al_2O_3 column filtration. The cross-linker *N*,*N*′-methylenebis(acrylamide) (BIS, Sigma-Aldrich, 99%) and the initiator 2,2′-azobis(2-methylpropionamidine) dihydrochloride (AMPA, Sigma-Aldrich, 97%) as well as the alkyl halides, and salts for the anion exchange were used as received. The used alkyl halides were namely: methyliodide, 1-bromododecane, and 1-bromohexadecane. All comonomers were synthesized in dimethylformamide (Sigma-Aldrich, >99.8%) and precipitated in p.a. diethylether (VWR chemicals, 100%). The used salts were sodium methanesulfonate (NaMeS, Sigma-Aldrich, 98%), sodium tetrafluoroborate ($NaBF_4$, Sigma-Aldrich, 98%), and bis(trifluoromethane) sulfonimide lithium salt ($LiNTf_2$, Sigma-Aldrich).

Synthesis of $VIM^+C_nH_{2n+1}[X]^-$ (n = 1, 12, 16) comonomers by quaternization of *N*-vinylimidazole *via* Menschutkin reaction with *n*-halidealkanes

The quaternized *N*-vinylimidazole derivatives with different alkyl chain length namely 1-vinyl-3-methylimidazolium iodide ($VIM^+C_1H_3[I]^-$), 1-vinyl-3-dodecanylimidazolium bromide

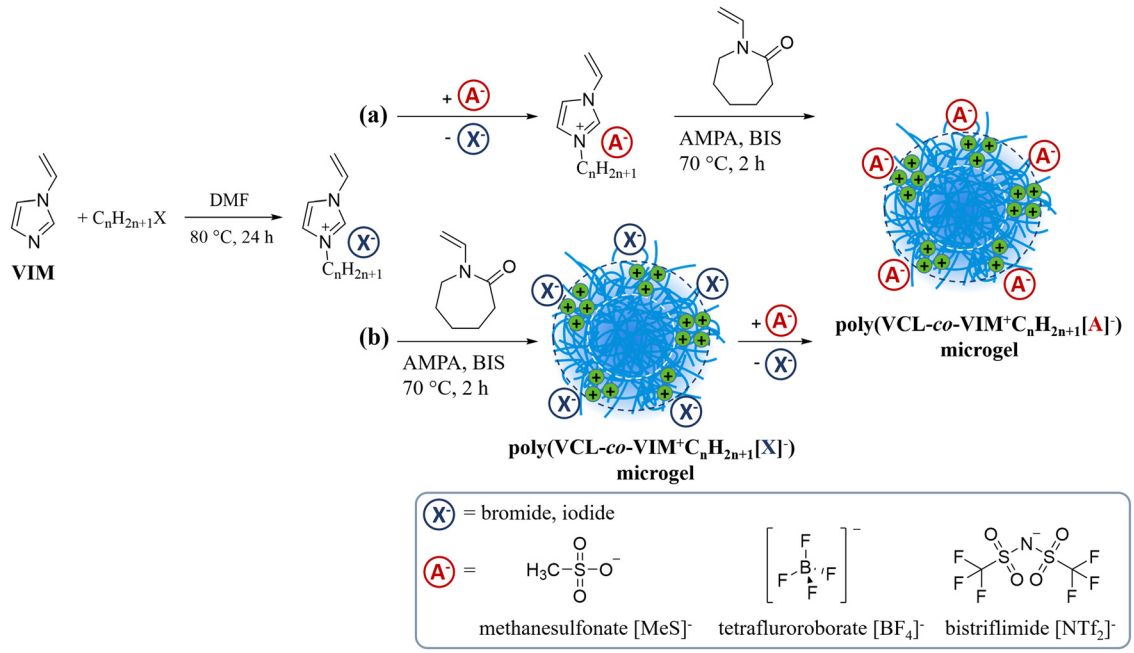

Scheme 1 Vinylimidazolium monomers are obtained from alkylation of *N*-vinylimidazole (VIM) with alkylhalides ($C_nH_{2n+1}X$). Poly(VCL-*co*-VIM$^+C_nH_{2n+1}$[A]$^-$) microgels with different counterions can be either accessed *via* (a) pre-functionalization of vinylimidazolium monomers with different counter anions (see legend) and subsequent copolymerization with *N*-vinylcaprolactam (VCL), or (b) post-modification of pre-synthesized poly(VCL-*co*-VIM$^+C_nH_{2n+1}$[X]$^-$) microgels with different anions. Both synthetic pathways and the properties of the resulting microgels are compared.

(VIM$^+C_{12}H_{25}$[Br]$^-$), and 1-vinyl-3-hexadecanylimidazolium bromide (VIM$^+C_{16}H_{33}$[Br]$^-$), were synthesized by general procedures described in ref. 7 and 28 with amounts given in ESI, Table S1.† The products were characterized by NMR spectroscopy and the respective spectra are presented in ESI, Fig. S1.†

Pre-functionalization of VIM$^+C_1H_3$[A]$^-$ comonomers by anion exchange

The anion exchange of the pre-synthesized VIM$^+C_1H_3$[I]$^-$ comonomer was performed by a general procedure described as follows. To a solution of vinylimidazolium iodide (2.5 mmol, 1 eq.) in water (20 mL), the respective anion salt (3.75 mmol, 1.5 eq.) was added (amounts see ESI, Table S2†). The resulting solution was stirred at room temperature overnight. Afterwards, the reaction mixture was lyophilized and the resulting solid was redispersed in dichloromethane to precipitate the sodium salt or lithium salt byproduct. The liquid phase was collected and the solvent was removed under reduced pressure. Characterization of the products, namely 1-vinyl-3-methylimidazolium methanesulfonate (VIM$^+C_1H_3$[MeS]$^-$), 1-vinyl-3-methylimidazolium tetrafluoroborate (VIM$^+C_1H_3$[BF_4]$^-$), and 1-vinyl-3-methylimidazolium bistriflimide (VIM$^+C_1H_3$[NTf_2]$^-$) was performed by Raman spectroscopy and NMR spectroscopy (see ESI†).

Pre-functionalization of VIM$^+C_nH_{2n+1}$[A]$^-$ (n = 12, 16) comonomers by anion exchange

The anion exchange on pre-synthesized VIM$^+C_nH_{2n+1}$[Br]$^-$ (n = 12, 16) comonomers was performed in a two-phase system. The comonomers (0.5 mmol, 1 eq.) were dissolved in 10 mL $CHCl_3$, while the respective salt (0.75 mmol, 1.5 eq.) was dissolved in 10 mL H_2O (amounts given in ESI, Table S2†). An emulsion of these two solutions was formed by adding them together, and then stirring vigorously for 24 h at room temperature. Afterwards, the organic and aqueous phase were separated and the organic phase was washed three times with fresh deionized water. The $CHCl_3$ was removed under reduced pressure and the obtained product was subsequently dried in a vacuum oven at T = 40 °C for 24 h. Characterization of the products, namely 1-vinyl-3-dodecanylimidazolium methanesulfonate (VIM$^+C_{12}H_{25}$[MeS]$^-$), 1-vinyl-3-dodecanylimidazolium tetrafluoroborate (VIM$^+C_{12}H_{25}$[BF_4]$^-$), and 1-vinyl-3-dodecanylimidazolium bistriflimide (VIM$^+C_{12}H_{25}$[NTf_2]$^-$), as well as 1-vinyl-3-hexadecanylimidazolium methanesulfonate (VIM$^+C_{16}H_{33}$[MeS]$^-$), 1-vinyl-3-hexadecanylimidazolium tetrafluoroborate (VIM$^+C_{16}H_{33}$[BF_4]$^-$), and 1-vinyl-3-hexadecanylimidazolium bistriflimide (VIM$^+C_{16}H_{33}$[NTf_2]$^-$) was performed by Raman spectroscopy and NMR spectroscopy (see ESI, Fig. S2 and S3†).

Synthesis of microgels containing halides as counterion

Poly(VCL-*co*-VIM$^+C_1H_3$[I]$^-$) microgels were synthesized from iodide-containing VIM$^+C_1H_3$ comonomer by batch precipitation polymerization as described in ref. 7. Poly(VCL-*co*-VIM$^+C_nH_{2n+1}$[Br]$^-$) microgels with n = 12, 16 were synthesized from bromide-containing VIM$^+C_nH_{2n+1}$ comonomers by semi-batch precipitation polymerization as described in ref. 28. The amount of functional ionic liquid comonomer was set to x = 10 mol% and the respective synthesis feed amounts are given in the ESI, Table S3.†

Synthesis of microgels from pre-functionalized $VIM^+C_nH_{2n+1}[A]^-$ (n = 1, 12, 16) comonomers

The pre-functionalized $VIM^+C_nH_{2n+1}[A]^-$ (n = 1, 12, 16) comonomers with either $[MeS]^-$, $[BF_4]^-$ or $[NTf_2]^-$ as counterion were applied in precipitation polymerization reactions with *N*-vinylcaprolactam (VCL) as main monomer. The concentrations of the respective comonomers were set to x = 10 mol% while the amount of cross-linker BIS was kept constant at x = 2 mol%, and the initiator AMPA at x = 0.6 mol% (amounts see ESI, Table S3†). The main monomer VCL and the cross-linker BIS were dissolved in 20 mL ultrapure H_2O and purged with N_2 for 30 min, while being heated to 70 °C and stirring. The syntheses using $VIM^+C_1H_3[A]^-$ comonomers were carried out in batch with the comonomer also added to VCL and BIS. Meanwhile, the initiator AMPA was dissolved in 2 mL ultrapure H_2O, and the respective $VIM^+C_nH_{2n+1}[A]^-$ comonomer was dissolved in 3 mL DMSO (in case of n = 12, 16). Both solutions were separately flushed with N_2 for 30 min at room temperature. By addition of the initiator solution to the heated mixture of VCL and BIS, the polymerization reaction was started. The respective $VIM^+C_nH_{2n+1}[A]^-$ comonomer (n = 12, 16) was added to the reaction mixture 3 min after the initiation, following an established protocol.[28] The reaction was allowed to proceed for 2 h at T = 70 °C while stirring. Afterwards, the resulting microgel dispersion was purified by dialysis for 4 days (MWCO = 12–14 kDa). The yield was determined by gravimetric analysis of a defined volume of microgel dispersion after lyophilization.

Post-functionalization of halide-containing microgels with anion salts

Aqueous microgel dispersions with a fix concentration of c = 10 mg mL^{-1} were prepared by dilution of the dispersions obtained after dialysis. To a volume of V = 10 mL the respective salt for the anion exchange was added. The amount of salt was calculated in regard to the comonomer concentration in the microgel and set to a ratio of 1 : 1 (n = 12, 16), and 1.5 : 1 (n = 1), respectively (amounts see ESI, Table S4†). The amount of comonomer in the microgel was determined by its mass fraction w_{VIM^+}, which is determined from the synthesis feed by

$$w_{VIM^+} = \frac{m_{VIM^+}}{m_{total}} \quad (1)$$

in which m_{VIM^+} defines the mass of the comonomer in the synthesis feed and m_{total} is the total mass of all reactants (monomers, cross-linker and initiator). The amount of salt n_{salt} was determined by

$$n_{salt} = n_{VIM^+} = \frac{m_{VIM^+,\,microgel}}{M_{VIM^+}} \quad (2)$$

with the mass of the comonomer within a given amount of microgel is given by $m_{VIM^+,\ microgel} = m_{microgel} \cdot w_{VIM^+}$, and the molar mass of the comonomer M_{VIM^+}.

After salt addition, the microgel sample was stirred vigorously overnight at room temperature to assure for complete anion exchange. The resulting water-soluble halide salt was removed by dialysis against 5 L of deionized water for 5 days in a regenerated cellulose membrane (MWCO = 12–14 kDa).

Differential scanning calorimetry (DSC)

Measurements were performed on a PerkinElmer DSC 8500 Differential Scanning Calorimeter equipped with CLN2 Controlled Liquid Nitrogen Accessory, fiber optical illuminator and an OmniCure S2000 light source. Approximately 10 mg of $VIM^+C_nH_{2n+1}[A]^-$ monomer or freeze-dried microgel were pressed in an aluminum pan and analyzed under N_2 atmosphere in the temperature range of −50–200 °C with a heating rate of 10 K min^{-1}. Results presented in the ESI, Fig. S4 and Table S5.†

Nuclear magnetic resonance (NMR) spectroscopy

^1H NMR spectra of $VIM^+C_nH_{2n+1}[A]^-$ comonomers were recorded using a NMR spectrometer Bruker DPX-400 FT-NMR. The samples were dissolved in DMSO-d_6 or $CDCl_3$ and measured at 300–400 MHz (^1H), 101 MHz (^{13}C), and 376 MHz (^{19}F) (see ESI†).

Raman spectroscopy

The presence of the counter ions $[A]^-$, as well as the incorporation of the $VIM^+C_nH_{2n+1}[A]^-$ commoners, was investigated by Raman spectroscopy on a Bruker RFS 100/S Raman spectrometer with a Nd:YAG laser, λ = 1064 nm. The comonomer powders or lyophilized microgel samples were pressed into an aluminum pan and measurements were carried out with a power of 200 mW, 1000 scans and spectral resolution of 4 cm^{-1}. The data was analyzed by OPUS 4.0 software.

Dynamic light scattering (DLS)

The DLS measurements were performed on a Zetasizer Ultra (Malvern Panalytical Ltd; UK) with microgel dispersions diluted with H_2O (LC-MS grade; Sigma-Aldrich) to diminish multiple scattering. Measurements for determination of the hydrodynamic diameter (D_h), polydispersity index (PDI) and temperature-dependent size change were performed. All measurements were performed with a fix scattering angle of θ = 90° and a laser beam operating at λ = 632.8 nm using a DTS0012 disposable cuvette. For all measurements 100 μL of the dialyzed microgel were diluted with 900 μL of ultrapure water. Temperature trends were measured in 5 K steps in the range of T = 10–60 °C with an equilibration time of 240 s at each temperature. For all reported values, an average of three measurements was taken and the corresponding standard deviation is presented as error bars. The software ZS Xplorer was used to analyze the results.

Electrophoretic light scattering (ELS)

The electrophoretic mobility was measured with a Zetasizer Ultra (Malvern Instruments, Germany) and a disposable capillary cell (DTS1070, Malvern Instruments GmbH). For all measurements 100 μL of the dialyzed microgel were diluted with 900 μL of ultrapure water. The solution was measured for

three times at T = 20–60 °C with an applied voltage of 150 V. The software ZS Xplorer was used to analyze the results.

Scanning transmission electron microscopy (STEM) and Scanning electron microscopy (SEM)

Electron microscopy images were recorded with an ultra-high resolution SU9000 cold field electron microscope (Hitachi) operating in SE or STEM mode. The microscope is equipped with a Wien filter to avoid electrostatic charging. Microgel samples were prepared from diluted microgel dispersions in water ($c \approx 1$ mg mL^{-1}) by droplet deposition on a carbonated Cu-grid. The solution was allowed to evaporate to ensure the complete drying of the sample before analysis. In case of poly (VCL-*co*-VIM$^+$C$_n$H$_{2n+1}$[NTf$_2$]$^-$) polymer residues (n = 1, 12) the samples were diluted in $CHCl_3$. The accelerating voltage is given in the figure captions.

Results and discussion

Microgel synthesis from pre-functionalized vinylimidazolium derivatives

Cationic amphiphilic ionic liquid VIM$^+$C$_n$H$_{2n+1}$[Br]$^-$ monomers were synthesized according to literature by alkylation of *N*-vinylimidazole (VIM) with variation of the alkyl chain length n = 12, 16. The successful synthesis of 1-vinyl-3-dodecylimidazolium bromide (VIM$^+$C$_{12}$H$_{25}$[Br]$^-$) and 1-vinyl-3-hexadecylimidazolium bromide (VIM$^+$C$_{16}$H$_{33}$[Br]$^-$) was proven by NMR.[28] In addition, a highly hydrophilic 1-vinyl-3-methylimidazolium derivative (VIM$^+$C$_1$H$_3$[I]$^-$) was synthesized by methylation of *N*-vinylimidazole with methyl iodide[3,7] to allow for comparison between short and long alkyl chain functionalization. These functional cationic comonomers bearing halides as counterions were applied in previous works for the generation of functional microgel carriers to be used in electrostatic interactions with oppositely charged payload.[3,28] Synthesis protocols to obtain functional microgels of low dispersity and narrow size distribution have been established for these alkyl chain lengths (batch or semi-batch), whereas variation of $1 < n < 12$ resulted in large heterogeneity and broad size distribution. As the vinylimidazolium comonomers possess ionic liquid properties, their physical and chemical properties are strongly dependent on the presence of counterions and the respective interionic interactions. In this context, the nature of the counterion can, *e.g.*, change the melting temperature of the ionic liquid and affect the solubility by changes in the hydrophobicity and interactions with water molecules. The melting temperature of amphiphilic halide containing comonomers is mainly dependent on the alkyl chain length, as an increase in crystallinity and thereby the melting temperature can be correlated to an increase in alkyl chain length.[28] In the present study, the comonomer properties were further studied as a function of the cation–anion interactions. For the pre-functionalization approach, these monomers were consequently applied in anion exchanges with methanesulfonate ([MeS]$^-$), tetrafluoroborate ([BF$_4$]$^-$), and bistriflimide ([NTf$_2$]$^-$). These anions were chosen because of their widely studied application in the formation of ionic liquids with divers resulting physical and chemical properties.[30–32] Strong deviations between the hydrogen bond accepting nature of the anions are reported in literature, which should alter the swelling behavior and overall properties of microgels synthesized thereof. Especially the application of the weakly coordinating anion [NTf$_2$]$^-$ should significantly influence the properties of the ionic liquids. The obtained comonomers already provided different physical states at room temperature, depending on the alkyl chain length, as well as on the type of counterion, ranging from viscous oils to powders. This observation was also analyzed by means of the melting temperatures (T_m) for all monomers, including the ones with halides as counterion, by differential scanning calorimetry (DSC) (see ESI, Table S5†). As expected, significant changes in the T_m were determined with regard to the present counterion, as well as the alkyl chain length. The overall dependency between the T_m and the present counterion at constant alkyl chain length can be established as follows [X]$^-$ > [MeS]$^-$ > [BF$_4$]$^-$ > [NTf$_2$]$^-$, which correlates with the cation–anion interaction strength and resulting lattice energy predicted by the Hofmeister series. All comonomers were also analyzed by Raman spectroscopy, which revealed the presence of the counterions by characteristic signals (exemplarily presented for VIM$^+$C$_{16}$H$_{33}$[A]$^-$ monomers in ESI, Fig. S3†). The reported bands are important reference data as they are detectable even in the microgel polymer network. In contrast, the presence of melting temperatures from poly(ionic liquid) compartments may be limited in the DSC analysis of microgels, as the attachment of the ionic liquid functionality to the polymer network restricts the flexibility and mobility of the alkyl chains and therefore limits the formation of crystalline domains.[28] Moreover, ^{1}H NMR measurements were conducted, which revealed the differences in cation–anion interactions for comonomers of the same alkyl chain length but different counterions by a signal shift of the aromatic C–H group of vinylimidazolium. Interionic interactions are mostly governed by the hydrogen bonds between the aromatic C–H groups and the respective anion. The most acidic C–H group, *i.e.*, the C3 position, is consequently the most important interaction side and the corresponding ^{1}H NMR signal will be affected the most by changes of the counterion. In this context, a lowfield shift of the signal can be correlated to stronger cation–anion interactions and therefore a more hydrogen bond accepting nature of the anion. The interionic interaction in, *e.g.*, VIM$^+$C$_{12}$H$_{25}$[A]$^-$ monomers (ESI, Fig. S2†) can be quantified qualitatively to be in the order [Br]$^-$ > [MeS]$^-$ > [BF$_4$]$^-$ > [NTf$_2$]$^-$. We have to mention that there is a difference in order within the Hofmeister series for bromide and iodide with the latter being more chaotropic in nature. However, the same order applies for iodide and bromide regarding the other employed anions. ^{19}F NMR spectra additionally proved the presence of the fluorinated anions tetrafluoroborate and bistriflimide. We should mention, that the introduction of tetrafluoroborate was achieved in a controlled way for n = 12, and 16, while it was only partially incor-

porated in $VIM^+C_1H_3$ monomer (4%). In the following we will nevertheless refer to it as $VIM^+C_1H_3[BF_4]^-$, which is justified by the fact, that already this partial exchange has a significant impact on the microgel properties. Further studies will focus on the improvement of the degree in tetrafluoroborate functionalization for $n = 1$.

The vinylimidazolium-based comonomers with different counter anions were employed in precipitation polymerization with *N*-vinylcaprolactam (VCL) as main monomer. *N*,*N*′-Methylenebis(acrylamide) (BIS) was used as cross-linker, and 2,2′-azobis(2-methylpropionamidine) dihydrochloride (AMPA) as initiator. The ratio of VCL and the comonomer was kept constant at $x = 10$ mol% $VIM^+C_nH_{2n+1}[A]^-$ to study the effect of the respective functional comonomer. The microgel syntheses were performed according to our established protocols for the incorporation of different cationic vinylimidazolium comonomers.[7,28] In brief, the incorporation of hydrophilic $VIM^+C_1H_3[I]^-$ is realized in a batch polymerization process, while the more hydrophobic vinylimidazolium derivatives are applied in a semi-batch approach with retarded addition of the comonomers dissolved in DMSO 180 s after the initiation. Both synthesis approaches will lead to a predominant localization of the charged comonomers in the corona region of the microgels. The employment of BIS as cross-linking agent will generally lead to the formation of a more cross-linked core and a less cross-linked more porous corona region owing to the different polymerization kinetics of VCL and BIS.[33–35] The solution behavior of these obtained reference microgel systems containing halides as counterions was analyzed by means of the temperature-dependent hydrodynamic diameter (D_h), and electrophoretic mobility (μ_E) (Fig. 1).

The size of the microgels in the swollen state, *i.e.*, at T = 20 °C, is dependent on the hydrophilicity of the employed vinylimidazolium comonomer. As expected, the C_1-functionalized comonomer resulted in an increased microgel size compared to the more hydrophobic comonomers, as well as non-functionalized PVCL microgel (Fig. 1(a), and Table 1). In addition, the temperature-induced decrease in microgel size and correlating volume phase transition temperature (VPTT) are strongly dependent on the hydrophilicity of the incorporated comonomer. While the C_{16}-functionalized microgel follows a typical sigmoidal decrease in hydrodynamic diameter with increasing temperature with a rather narrow width of transition, the C_1-functionalized microgel is characterized by an almost linear decrease in size with a broad transition and high VPTT. The corresponding VPTTs were determined from sigmoidal Boltzmann fit functions of the DLS data and showed a decrease from $T_{VPT}(VIM^+C_1H_3[I]^-)$ = 44.7 ± 1.6 °C (R^2 = 0.978) to $T_{VPT}(VIM^+C_{16}H_{33}[Br]^-)$ = 31.5 ± 0.4 °C (R^2 = 0.995). All poly(VCL-*co*-$VIM^+C_nH_{2n+1}[X]^-$) microgels (n = 1, 12, 16) have a small size distribution, which was determined by means of the polydispersity index (PDI) using DLS (Table 1).

Additionally, the electrophoretic mobility of the halide-containing microgels was analyzed in the process of temperature-induced volume phase transition (Fig. 1(b)). Reference poly(*N*-vinylcaprolactam) microgels without functional comonomer

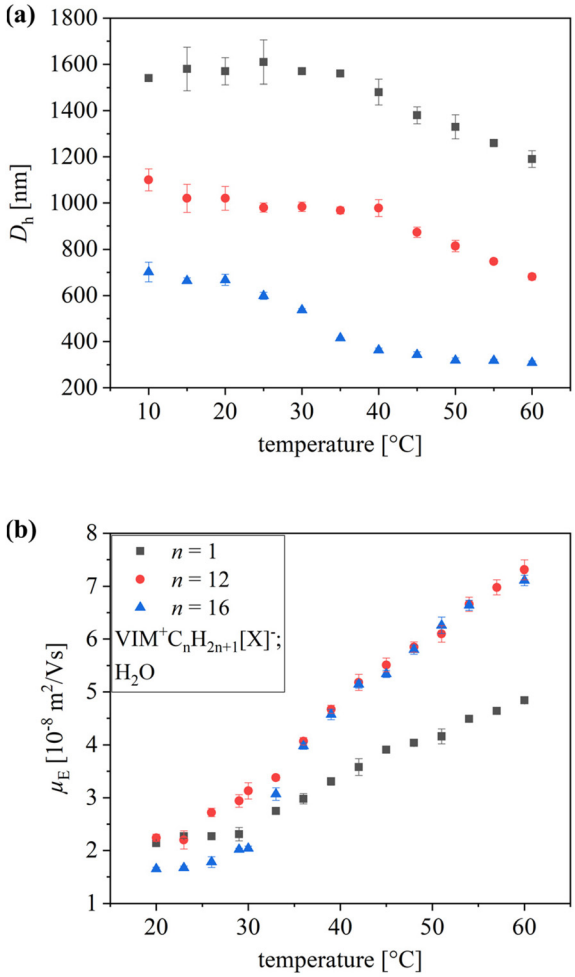

Fig. 1 (a) Hydrodynamic diameter (D_h), and (b) electrophoretic mobility (μ_E) of poly(VCL-*co*-$VIM^+C_nH_{2n+1}[X]^-$) microgels as a function of alkyl chain length, and temperature (n = 1, black squares; n = 12, red dots; n = 16, blue triangles).

can possess a negligible electrophoretic mobility[3] (here: μ_E 20 °C = 0.19 ± 0.01 × 10^{-8} m^2 V^{-1} s^{-1}), which results from the incorporated initiator residue. While the electrophoretic mobility of solid nanoparticles is limited by the zeta potential, *i.e.*, the surface charge of the particle (Smoluchowski's model), it is more complex in the context of partially ion-penetrable microgels (Ohshima's model).[36] Thus, the electrophoretic mobility was found to be affected by the alkyl chain length attached to the cationic comonomer in the swollen state (T = 20 °C) with a decreased μ_E for n = 16, compared to n = 1, 12, which could be attributed to a shielding effect of the hydrophobic alkyl chains by their increased crystallinity. In contrast, the electrophoretic mobility in the collapsed state (T = 60 °C) was determined to be similar for n = 12, 16, but significantly smaller for n = 1. A possible explanation is a difference in the location of the cationic vinylimidazolium comonomers within the corona of the microgels.

The application of tetrafluoroborate ($[BF_4]^-$), and methanesulfonate ($[MeS]^-$) containing ionic liquid comonomers at a

Table 1 Hydrodynamic diameter (D_h) and polydispersity indices (PDIs) of poly(VCL-*co*-VIM$^+$C$_n$H$_{2n+1}$[A]$^-$) microgels from pre-functionalization (n = 1, 12, 16) measured in H_2O at T = 20 °C and 60 °C by DLS

Microgel sample	D_h 20 °C [nm]	PDI 20 °C [a. u.]	D_h 60 °C [nm]	PDI 60 °C [a. u.]
PVCL-ref.	988 ± 45	0.093 ± 0.078	407 ± 5	0.055 ± 0.017
VIM$^+$C$_1$H$_3$[I]$^-$	1570 ± 59	0.046 ± 0.059	1190 ± 36	0.039 ± 0.044
VIM$^+$C$_{12}$H$_{25}$[Br]$^-$	1020 ± 52	0.108 ± 0.020	682 ± 14	0.020 ± 0.028
VIM$^+$C$_{16}$H$_{33}$[Br]$^-$	668 ± 24	0.125 ± 0.045	309 ± 7	0.112 ± 0.019
VIM$^+$C$_1$H$_3$[MeS]$^-$	1430 ± 15	0.020 ± 0.012	916 ± 8	0.040 ± 0.046
VIM$^+$C$_{12}$H$_{25}$[MeS]$^-$	787 ± 14	0.035 ± 0.022	481 ± 2	0.072 ± 0.019
VIM$^+$C$_{16}$H$_{33}$[MeS]$^-$	668 ± 28	0.089 ± 0.067	298 ± 6	0.066 ± 0.033
VIM$^+$C$_1$H$_3$[BF$_4$]$^-$	693 ± 20	0.091 ± 0.037	542 ± 3	0.121 ± 0.020
VIM$^+$C$_{12}$H$_{25}$[BF$_4$]$^-$	633 ± 28	0.139 ± 0.048	326 ± 7	0.028 ± 0.006
VIM$^+$C$_{16}$H$_{33}$[BF$_4$]$^-$	597 ± 8	0.076 ± 0.030	281 ± 2	0.042 ± 0.006

degree of functionalization of x = 10 mol% let to the formation of stable, turbid microgel dispersions, which were purified by dialysis after the synthesis. The microgel yield was determined by gravimetric analysis of lyophilized microgel and was found to be mainly dependent on the applied counterion. Similar to the ionic liquid monomers, the obtained pre-functionalization poly(VCL-*co*-VIM$^+$C$_n$H$_{2n+1}$[A]$^-$) microgels were analyzed using Raman spectroscopy and showed the characteristic signals found in the pre-functionalized comonomers (ESI, Fig. S5†). Moreover, the microgels obtained from VIM$^+$C$_n$H$_{2n+1}$[BF$_4$]$^-$ and VIM$^+$C$_n$H$_{2n+1}$[MeS]$^-$ comonomers show a low dispersity, which was determined by DLS for different temperatures, *i.e.*, the swollen state at T = 20 °C and collapsed state at T = 60 °C (Table 1). The surfactant properties of the comonomers and the competing functionalities, *i.e.*, the repulsion of the positive charges and the attractive hydrophobic interactions between the alkyl chains, will lead to an increased heterogeneity of the polymer network. In addition, the incorporation of charged comonomers in the linear polymer chains during microgel formation will strongly affect the solubility and corresponding volume phase transition temperature of these polymer chains. As the collapse of the polymer chains is mandatory for the formation of precursor microgels and subsequent growth thereof, the incorporation of cationic comonomers by precipitation polymerization with control of concentration and high yield is limited.[6,37] Consequently, the degree of functionalization was kept constant at a moderate value of x = 10 mol% in this work. Interestingly, the employment of [NTf$_2$]$^-$ containing comonomers in the microgel synthesis resulted in almost complete precipitation of formed microgels in the aqueous reaction medium. The presence of this weakly coordinating anion significantly decreased the hydrophilicity of the comonomer and formed microgels, respectively. The poly(VCL-*co*-VIM$^+$C$_n$H$_{2n+1}$[NTf$_2$]$^-$) residues were dissolved in $CHCl_3$ and analyzed by electron microscopy to verify the formation of microgels despite the loss in colloidal stability (Fig. 2(j) and (k)). While polymeric aggregates were found for the poly(VCL-*co*-VIM$^+$C$_1$H$_3$[NTf$_2$]$^-$) synthesis (Fig. 2(j)), defined spherical colloids of low dispersity were found for the C$_{12}$-functionalized comonomer (Fig. 2(k)). It can be concluded that the decrease in solubility strongly limits the control of the microgel formation and comonomer incorporation but can lead to microgels of spherical shape in case of VIM$^+$C$_{12}$H$_{25}$[NTf$_2$]$^-$ comonomer. Further investigation and improvement of the microgel synthesis *via* pre-functionalization with bistriflimide is required for the controlled generation of poly(VCL-*co*-VIM$^+$C$_n$H$_{2n+1}$[NTf$_2$]$^-$) microgels using this synthesis approach.

The incorporation of the pre-functionalized vinylimidazolium comonomers, *i.e.*, the presence of the respective anions and attached alkyl chain is expected to influence the solution and swelling behavior of microgels. In addition, we hypothesized that the presence of vinylimidazolium comonomers may also alter the morphology of the microgels. Therefore, electron microscopy images were conducted of all microgel samples generated by the pre-functionalization approach (Fig. 2). The reference microgels synthesized from halide-containing vinylimidazolium comonomers exhibit a spherical shape and a narrow size distribution. A core–corona morphology can be assumed for poly(VCL-*co*-VIM$^+$C$_{12}$H$_{25}$[Br]$^-$) and poly(VCL-*co*-VIM$^+$C$_{16}$H$_{33}$[Br]$^-$) microgels, which is supported by our previous studies.[28] Overall, the poly(VCL-*co*-VIM$^+$C$_{16}$H$_{33}$[A]$^-$) microgels are least affected by the presence of different counterions from pre-functionalization. As depicted in Fig. 2(c), (f), and (i) no significant morphology changes can be correlated with the type of present counterion. In contrast, the poly(VCL-*co*-VIM$^+$C$_1$H$_3$[A]$^-$) microgels are characterized by the formation of a more diffuse corona in case of methanesulfonate as counterion (Fig. 2(d)). A change in contrast and correlated decrease in microgel polymer network stiffness can be assumed for the poly(VCL-*co*-VIM$^+$C$_{12}$H$_{25}$[MeS]$^-$) microgels (Fig. 2(e)). The most prominent and remarkable anion-induced morphology change was found for the poly(VCL-*co*-VIM$^+$C$_{12}$H$_{25}$[BF$_4$]$^-$) microgels as depicted in Fig. 2(h). These microgels are characterized by an anisotropic shape with defined spherical domains, which are connected to a larger core domain. The diameter of the domains was determined as D = 151 ± 18 nm (from 100 counts) and each microgel contains 4–6 such domains. SEM images further confirmed the anisotropic but regular structure of these microgels compared to non-functionalized pure PVCL microgels (ESI, Fig. S6†).

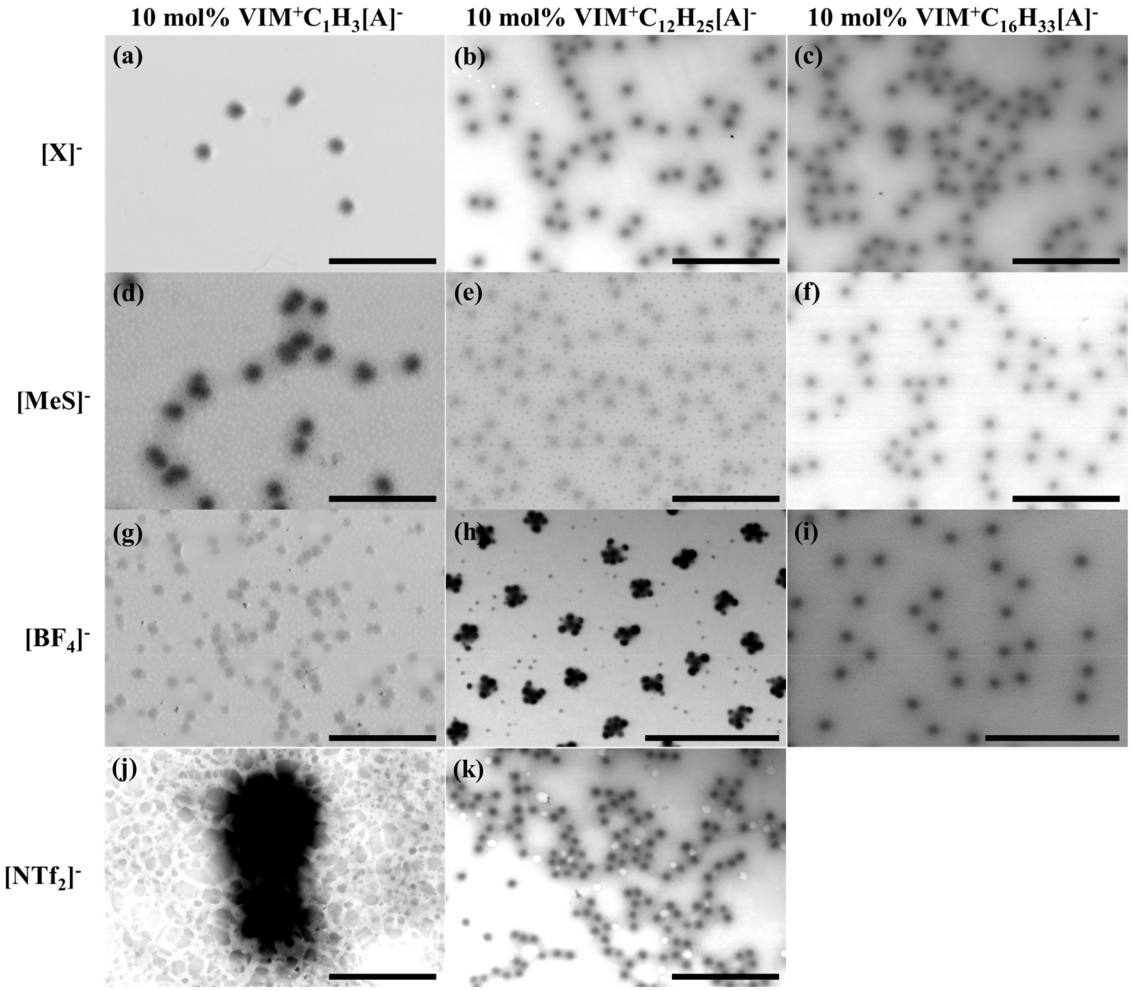

Fig. 2 BFSTEM images of poly(VCL-*co*-VIM$^+$C$_n$H$_{2n+1}$[A]$^-$) microgels (n = 1, 12, 16) with x = 10 mol%. Images (a)–(c) represent the microgels containing halides as counterion, (d)–(f) represent methanesulfonate functionalized microgels, (g)–(i) show tetrafluoroborate containing microgels, and (j)–(k) present polymeric residues from application of bistriflimide containing comonomers. Scale bar is set to 2 μm and accelerating voltage is 30.0 kV.

Similar formation of anisotropic microgel morphologies as a function of the comonomer concentration was recently reported in our group using hydrophobic bis(pyrazolyl) methacrylate comonomers and VCL in semi-batch precipitation polymerization.[16] We assume that this unusual microgel morphology is formed by the controlled aggregation of growing microgel precursors. However, more systematic investigations of the microgel formation mechanism employing, *e.g.*, *in situ* DLS, SANS or SAXS measurements, are needed to clarify the formation of the nano-domain structure.

Behavior of pre-functionalized poly(VCL-*co*-VIM$^+$C$_n$H$_{2n+1}$[A]$^-$) microgels in H$_2$O

While high charge density can contribute to pronounced hydrophilicity reflected by an increase of the VPTT, the presence of charges can also limit the polymer network flexibility as demonstrated for hydrophilic poly(VCL-*co*-VIM$^+$C$_1$H$_3$[I]$^-$) microgels.[7] Thus, the temperature-induced decrease in volume can be limited in case of highly charged microgels.[38,39] In addition, the temperature-dependent behavior can be altered by the alkyl chain length and present counterion. The swelling behavior of the [MeS]$^-$ and [BF$_4$]$^-$-functionalized microgels with different alkyl chain lengths and constant degree of functionalization x = 10 mol% was studied as a function of temperature to investigate the influence of the counterion on characteristic microgel properties such as hydrodynamic diameter (D_h) and VPTT (Fig. 3). Significant differences in the temperature-induced decrease in D_h can be observed. Overall, the pre-functionalized poly(VCL-*co*-VIM$^+$C$_n$H$_{2n+1}$[A]$^-$) microgels (n = 1, 12, 16) show a decrease in size in the order [X]$^-$ > [MeS]$^-$ > [BF$_4$]$^-$ (see Table 1). This observation can be explained by the Hofmeister series, which indicates an increase in chaotropic nature in this order leading to the disturbance of ordered hydrogen bonds and thus, less swelling. In this context, the difference in size between halide-functionalized and methanesulfonate-functionalized microgel is less

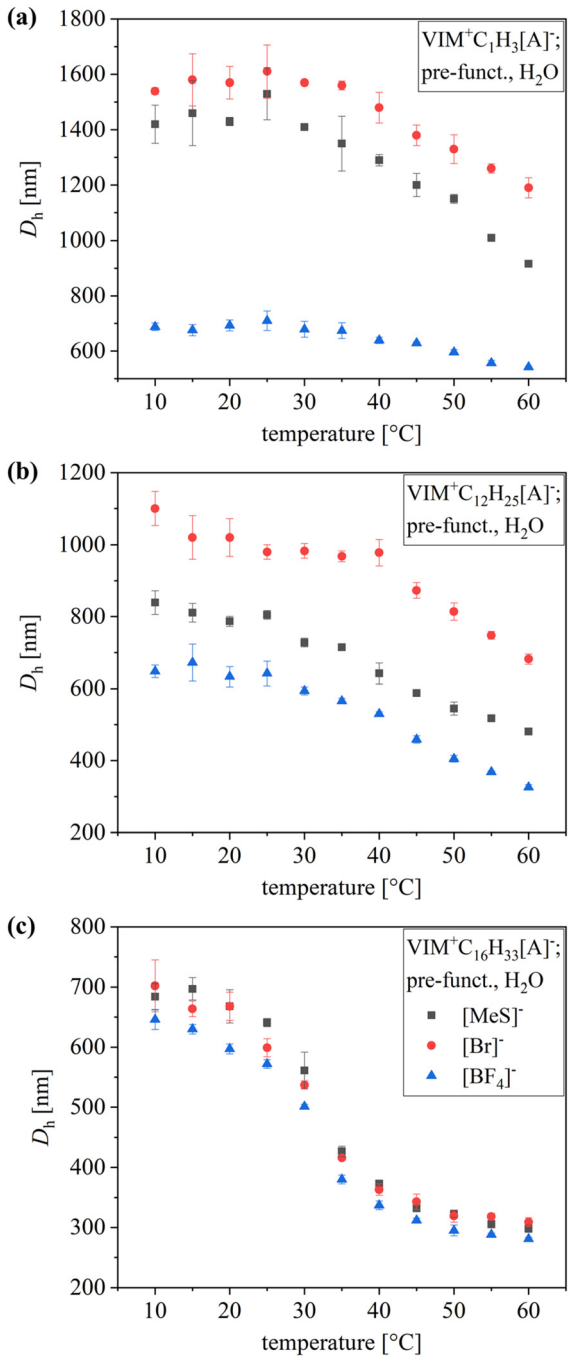

Fig. 3 Hydrodynamic diameter (D_h) as a function of alkyl chain length, counterion and temperature of pre-functionalized microgels. Temperature-dependent D_h of (a) $VIM^+C_1H_3[A]^-$ microgels, (b) $VIM^+C_{12}H_{25}[A]^-$ microgels, and (c) $VIM^+C_{16}H_{33}[A]^-$ microgels with different counter anions.

pronounced for poly(VCL-*co*-$VIM^+C_nH_{2n+1}[A]^-$) microgels with n = 1, than for n = 12. This result is in line with the difference in kosmotropic behavior of bromide and iodide anion with the latter being more similar to methanesulfonate. It is striking that similar sizes were measured for poly(VCL-*co*-$VIM^+C_nH_{2n+1}[BF_4]^-$) microgels with n = 1, 12 and 16 in the swollen state (D_h = 700–600 nm) with only a small impact of the increasing alkyl chain length and accompanied hydrophobicity. A possible explanation can be the aforementioned only partial exchange with tetrafluoroborate in case of n = 1. However, the temperature-dependent decrease in size showed significant differences with a less hydrophobic microgel nature, *e.g.*, C_{12}-alkyl chain, resulting in flat, less sigmoidal, curves and higher VPTTs. Precisely, the volume phase transition temperature was determined by sigmoidal Boltzmann fit functions to be decreasing from $T_{VPT}(VIM^+C_1H_3[BF_4]^-)$ = 49.1 ± 1.7 °C (R^2 = 0.993) to $T_{VPT}(VIM^+C_{16}H_{33}[BF_4]^-)$ = 31.9 ± 0.5 °C (R^2 = 0.999). The poly(VCL-*co*-$VIM^+C_{16}H_{33}[A]^-$) microgels are least affected by the type of counterion present with regard to their size in swollen and collapsed state, as well as the VPTT (T_{VPT} ≈ 32 °C; R^2 = 0.996). These results from DLS measurements support the impression of anion-independent microgel formation derived from the electron microscopy images (Fig. 2(c), (f) and (i)).

Additionally, the temperature-dependent electrophoretic mobility (μ_E) of the pre-functionalized poly(VCL-*co*-$VIM^+C_nH_{2n+1}[A]^-$) microgels (n = 1, 12, 16) was determined by electrophoretic light scattering (ELS) to study the effect of the alkyl chain length and present anion. In previous studies we could demonstrate, that the temperature-induced change in μ_E can be correlated with the collapse of the cationic microgels upon temperature increase.[7,28] As the microgels become more rigid and compact, their electrophoretic mobility increases and can reach a maximum surface charge density. Consequently, the μ_E is expected to follow similar trends as the temperature-dependent swelling behavior depicted in Fig. 3. As listed in Table 2, the halide-functionalized microgels overall show the highest electrophoretic mobilities in the swollen state (T = 20 °C). The hydrodynamic diameter of C_{16}-functionalized microgels was found to be almost not affected by the type of present counterion, which is also supported by similar μ_E values for methanesulfonate and tetrafluoroborate. In a similar fashion, the microgels with n = 1 show a decrease in electrophoretic mobility with decreasing size in the swollen state.

Table 2 Electrophoretic mobilities (μ_E) of poly(VCL-*co*-$VIM^+C_nH_{2n+1}[A]^-$) microgels (n = 1, 12, 16) from pre-functionalization, measured in H_2O at T = 20 °C and 60 °C

Microgel sample	μ_E 20 °C [10^{-8} m^2 V^{-1} s^{-1}]	μ_E 60 °C [10^{-8} m^2 V^{-1} s^{-1}]
$VIM^+C_1H_3[I]^-$	2.14 ± 0.03	4.84 ± 0.05
$VIM^+C_{12}H_{25}[Br]^-$	2.24 ± 0.07	7.31 ± 0.19
$VIM^+C_{16}H_{33}[Br]^-$	1.65 ± 0.03	7.11 ± 0.10
$VIM^+C_1H_3[MeS]^-$	2.02 ± 0.16	5.74 ± 0.02
$VIM^+C_{12}H_{25}[MeS]^-$	1.08 ± 0.11	7.03 ± 0.34
$VIM^+C_{16}H_{33}[MeS]^-$	0.91 ± 0.03	6.78 ± 0.04
$VIM^+C_1H_3[BF_4]^-$	1.61 ± 0.23	4.04 ± 0.25
$VIM^+C_{12}H_{25}[BF_4]^-$	1.59 ± 0.14	6.81 ± 0.14
$VIM^+C_{16}H_{33}[BF_4]^-$	1.06 ± 0.14	6.99 ± 0.15

Characterization of post-functionalized poly(VCL-*co*-VIM$^+$C$_n$H$_{2n+1}$[A]$^-$) microgels

The post-functionalization of pre-synthesized poly(VCL-*co*-VIM$^+$C$_n$H$_{2n+1}$[X]$^-$) microgels (n = 1, 12, 16) bearing halides as counterion, was performed by adding the respective salt containing the counterion [A]$^-$ to the microgel dispersion and stirring overnight followed by dialysis against deionized water. This experimental procedure has already been used for anion exchange on ionic liquid homopolymers as reported in literature.[40,41] In contrast to the linear poly(ionic liquids), the microgels are challenging in the context of anion exchange. While the outer sphere of the microgels can be considered as permeable open-pore structure that allows for diffusion of ions, the more cross-linked core region may limit the exchange of ions. As the vinylimidazolium comonomer incorporation was controlled in the case of VIM$^+$C$_{12}$H$_{25}$[Br]$^-$ and VIM$^+$C$_{16}$H$_{33}$[Br]$^-$ with a predominant localization in the less cross-linked corona, the entrapment of bromide ions should be negligible. Counter wise, the network structure of the microgels could lead to an entrapment of added anions even if no opposing charges are present. Consequently, a reference PVCL microgel sample with no incorporated cationic comonomer was treated with the same amount of salt and purified by dialysis to prove the successful removal of anions in the absence of positive charges. As demonstrated by Raman spectroscopy and DLS measurements, the PVCL reference microgel was not affected by the salt treatment (see ESI, Fig. S7†).

Poly(VCL-*co*-VIM$^+$C$_n$H$_{2n+1}$[A]$^-$) microgels samples (n = 1, 12, 16) were lyophilized to perform Raman spectroscopy in order to prove the presence of the respective counter anion (ESI, Fig. S8†). All applied counter anions can be identified by characteristic vibrations present in the microgel spectra. In addition, the successful exchange of the counter anion was proven by ^{19}F NMR in case of bistriflimide and tetrafluoroborate showing the characteristic signals, which were also observed for the pre-modified comonomers.

The effect of the present counter anion was determined by means of the hydrodynamic diameter (D_h) of the microgels as a function of temperature, as well as the electrophoretic mobility (μ_E), and the melting temperature of poly(ionic liquid) compartments within the microgels. The latter was found to be only detectable for C$_{16}$-microgels, which is in line with our previous studies.[28] A covalent attachment of the cationic charges and alkyl chains to the polymer network will limit the flexibility for the formation of large crystalline domains. Therefore, a long alkyl chain is required for the generation of detectable melting transitions (see ESI, Fig. S9†). As the post-functionalization will not change the microgel precursor by means of its inherent morphology, the presence of the counterions should clearly affect the determined characteristics as a function of the cation–anion interaction strength, as well as the anion hydrophobicity. It should be mentioned that the amount of salt (n [mol]) was constant in all cation exchange experiments and was calculated with regard to the incorporated amount of vinylimidazolium comonomer (see eqn (1) and (2)). The hydrodynamic diameters and polydispersity indices determined by DLS are given in Table 3. Independently of the present counter anion, the D_h in swollen and collapsed state was found to be influenced by the hydrophilicity of the alkyl chain length of the cationic comonomer. A decrease in size was observed in the order C$_1$ > C$_{12}$ > C$_{16}$. In addition, the nature of the anion affects the microgel size and swelling with an increase in size by the addition of methanesulfonate and a decrease in size by functionalization with tetrafluoroborate, respectively.

A comparison of the hydrodynamic diameters of pre- and post-functionalized microgels containing the same anion (compare Tables 1 and 3) reveals a difference in size, which is affected by the alkyl chain length of the cationic comonomer. Precisely, the methanesulfonate-functionalized microgels are significantly smaller following the pre-functionalization approach in case of n = 1, 12 but approximately similar in size for n = 16. Similar dependencies were determined for tetrafluoroborate-functionalized microgels, *i.e.*, the post-functionalized microgels of n = 12, 16 are larger in size, than the pre-functionalized pendants.

Bistriflimide addition in the post-functionalization approach led to the agglomeration of microgels. Therefore, the quality of data obtained for these samples by DLS is limited and not reported in Table 3.

The electrophoretic mobility of the post-functionalization approach was found to be dependent on both the alkyl chain length, and the counterion in the swollen state (Fig. 4(a) and (c)). The most prominent effect of the counter anion was determined for the VIM$^+$C$_{12}$H$_{25}$-10 microgels indicating that the cation–anion interaction has a more significant impact in this system. Differences in the μ_E were already present in the

Table 3 Hydrodynamic diameter (D_h) and polydispersity indices (PDIs) of poly(VCL-*co*-VIM$^+$C$_n$H$_{2n+1}$[A]$^-$) microgels from post-functionalization (n = 1, 12, 16) measured in H$_2$O at T = 20 °C and 60 °C by DLS

Microgel sample	D_h 20 °C [nm]	PDI 20 °C [a. u.]	D_h 60 °C [nm]	PDI 60 °C [a. u.]
VIM$^+$C$_1$H$_3$[MeS]$^-$	1750 ± 93	0.148 ± 0.008	1370 ± 18	0.037 ± 0.025
VIM$^+$C$_{12}$H$_{25}$[MeS]$^-$	997 ± 69	0.107 ± 0.045	651 ± 19	0.049 ± 0.010
VIM$^+$C$_{16}$H$_{33}$[MeS]$^-$	694 ± 13	0.129 ± 0.010	362 ± 9	0.130 ± 0.024
VIM$^+$C$_1$H$_3$[BF$_4$]$^-$	1430 ± 1	0.141 ± 0.079	1260 ± 19	0.055 ± 0.012
VIM$^+$C$_{12}$H$_{25}$[BF$_4$]$^-$	841 ± 33	0.202 ± 0.030	359 ± 1	0.117 ± 0.011
VIM$^+$C$_{16}$H$_{33}$[BF$_4$]$^-$	631 ± 20	0.124 ± 0.015	313 ± 6	0.074 ± 0.044

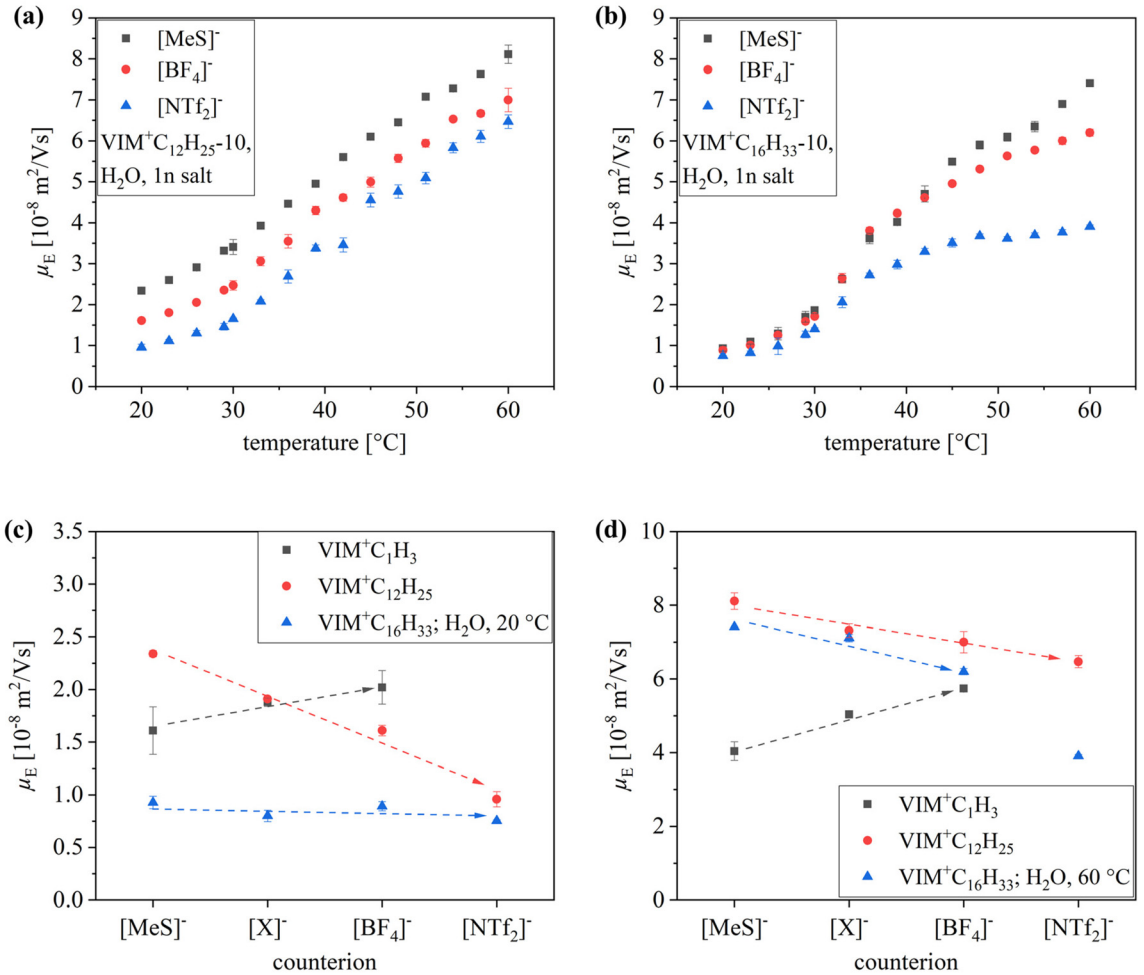

Fig. 4 Electrophoretic mobility (μ_E) as a function of alkyl chain length, counterion and temperature of post-functionalized microgels. Temperature-dependent μ_E of (a) $VIM^+C_{12}H_{25}$ microgels, and (b) $VIM^+C_{16}H_{33}$ microgels with different counterions. Comparison of μ_E for different alkyl chain lengths and counterions at (c) T = 20 °C, and (d) T = 60 °C. Dotted arrows are a guide to the eye.

swollen state of the microgels (T = 20 °C) and remained similar throughout the temperature-induced collapse (Fig. 4(a)). In the presence of $[MeS]^-$, the electrophoretic mobility is even increased compared to the reference system with $[Br]^-$ as counterion from 1.91 ± 0.01 × 10^{-8} m^2 V^{-1} s^{-1} to 2.34 ± 0.03 × 10^{-8} m^2 V^{-1} s^{-1}. A less significant increase was determined for the $VIM^+C_{16}H_{33}$-10 microgels. Overall, the determined electrophoretic mobilities of the post-functionalized $VIM^+C_{16}H_{33}$-10 microgels were less affected by the exchange of the counterion. As depicted in Fig. 4(b), the μ_E determined in the swollen state of the microgels (T = 20 °C) was almost equal for all counterions. It can be concluded, that the effective surface charge is only determined by the amount of present anions regardless of the strength in cation–anion interaction. In contrast, the temperature-dependent change in electrophoretic mobility, which is induced by the collapse of the microgels and resulting increased surface charge density, shows strong deviations in case of the $VIM^+C_{16}H_{33}$-10 microgels regarding different counterions. The effect of the different counterions in the swollen state as a function of the alkyl chain length follows significantly different trends as depicted in Fig. 4(c). While the $VIM^+C_{12}H_{25}$-10 microgel shows a decrease in electrophoretic mobility in the order $[MeS]^-$ > $[Br]^-$ > $[BF_4]^-$ > $[NTf_2]^-$, an opposite trend is observed for the $VIM^+C_1H_3$-10 microgels and almost no change in μ_E is determined for the $VIM^+C_{16}H_{33}$-10 microgels. These findings might result from differences not only in the cation–anion interaction strength, but also in the microgel network permeability and confined location of the positive charges within the microgel network. Further investigations are required for the validation of this hypothesis.

When measured in the collapsed states (T = 60 °C), the electrophoretic mobilities were observed to be less affected by the alkyl chain length ranging from, *e.g.*, 7.31 ± 0.2 × 10^{-8} m^2 V^{-1} s^{-1} (C_{12}) to 7.11 ± 0.1 × 10^{-8} m^2 V^{-1} s^{-1} (C_{16}) for bromide as counterion. Again, the highest electrophoretic mobility was found for $VIM^+C_{12}H_{25}$-10$[MeS]^-$ while all samples with $[NTf_2]^-$ as counterion provided the lowest electrophoretic mobility. The approximation of the values determined for the collapsed state suggests that the effect of the cation–anion interaction is especially dominant in the swollen state when the microgels

act as soft polymers. This observation can be explained by the complex cation–anion interactions in case of a partially permeable microgel network. The allocation of the counterions in a mobile or stationary region of the microgel and penetration inside the microgel network can strongly influence the effective surface charge. This complex behavior will presumably be governed by the cation–anion interaction strength, the accessibility of the cationic charges within the microgel network, as well as the size of the anions. In the collapsed state the microgels act distinctly more like rigid spherical polymer particles. Thus, the effective surface charge is less affected by differences in the microgel network porosity and anion diffusion but mainly governed by the cation–anion interactions. These will lead to more similar electrophoretic mobilities with regard to the alkyl chain length. In this context, further investigations could focus on studies of the allocation of the anions within the microgel network, *e.g.*, by high-resolution NMR and diffusometry.

Solution behavior of poly(VCL-*co*-VIM$^+$C$_n$H$_{2n+1}$[A]$^-$) microgels at increased ionic strength

The effective surface charge, *i.e.*, electrophoretic mobility, and swelling degree of microgels carrying pH-independent charges can be controlled by a change in ionic strength. An increase in ionic strength will lead to a decreased solubility of the polymer network, which is accompanied by less swelling and a significant decrease of the volume phase transition temperature. In addition, the stabilizing effect and osmotic pressure induced by the charges will decrease leading to aggregation at high ionic strength, *i.e.*, high salt concentration,[42] and further decrease in swelling.[38,39] The hydrophilic poly(VCL-*co*-VIM$^+$C$_1$H$_3$[I]$^-$) microgel shows the highest solubility in aqueous solution and tolerates even an ionic strength of I = 100 mM without aggregation upon heating (Fig. 5(a)). Nevertheless, a strong decrease in size with increasing ionic strength, *e.g.*, from $D_{h,1\ mM}$ (20 °C) = 873 ± 18 nm to $D_{h,1\ M}$ (20 °C) = 469 ± 3.7 nm, and a shift of the VPTT can be observed. Aggregation was only determined at the highest ionic strength (I = 1 M) for T > 20 °C.

Since studies in literature report the occurrence of UCST-like solution behavior of typically LCST-type cationic polymer materials in solution of increased ionic strength[43] and presence of halides,[19,20] the temperature-dependent swelling of the poly(VCL-*co*-VIM$^+$C$_n$H$_{2n+1}$[A]$^-$) microgels was also studied in 10 mM NaCl-solution. The use of NaCl in temperature-dependent measurements is justified by the almost temperature-independent solubility of NaCl in water and thus, constant ionic strength of the solution. The microgels functionalized by hydrophobic alkyl chains were found to be less stable in solution of increased ionic strength compared to the microgels containing methylated vinylimidazolium. Nevertheless, the decrease in hydrodynamic diameter (in the swollen state) was proven for all microgel samples, as expected. In addition, the introduction of different counterions by pre- or post-functionalization led to aggregation of the microgels upon heating in I = 10 mM (exemplarily demonstrated for poly(VCL-*co*-VIM$^+$C$_{16}$H$_{33}$[BF$_4$]$^-$) microgels; see ESI, Fig. S10(a)†). Thus, the presence of the applied anions leads to a significant decrease in both solubility and stabilization by the charges. The only exception was found for the anisotropic poly(VCL-*co*-VIM$^+$C$_{12}$H$_{25}$[BF$_4$]$^-$) microgel sample synthesized *via* pre-functionalization of the comonomer. While the post-functionalized microgel sample of the same composition showed aggregation for T > 30 °C, the pre-functionalized microgel is characterized by a first similar decrease in hydrodynamic diameter, which is followed by a re-swelling for T > 30 °C (Fig. 5(b)). While aggregation is reflected in a size jump and increase in PDI, this microgel sample shows no increase in PDI.

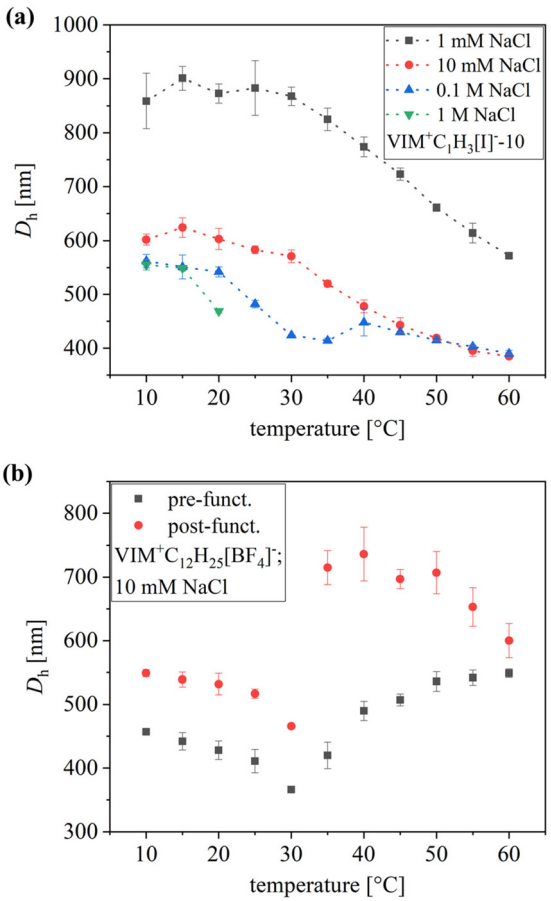

Fig. 5 Hydrodynamic diameter (D_h) as a function of temperature for (a) poly(VCL-*co*-VIM$^+$C$_1$H$_3$[I]$^-$) microgels x = 10 mol% at different ionic strength, and (b) of poly(VCL-*co*-VIM$^+$C$_{12}$H$_{25}$[BF$_4$]$^-$) microgels (x = 10 mol%) from pre- and post-functionalization approach measured in aqueous 10 mM NaCl solution. Dotted lines are a guide to the eye.

Possible explanations are the stabilizing effect of the effective surface charge of the microgels, which was reported before to be dependent on the alkyl chain length at the same degree of functionalization.[28] Consequently, the VIM$^+$C$_{12}$H$_{25}$[BF$_4$]$^-$ monomer would have a pronounced stabilizing effect in solution of increased ionic strength. In addition, the cation–anion interaction was also found to be affected by the alkyl chain length. As the microgels functionalized by n = 12 were found to possess an anisotropic mor-

phology this feature could further promote the second volume phase transition. In this context, the changes in hydrodynamic diameter could refer to the collapse of the mostly PVCL-containing core, followed by swelling of the poly(ionic liquid)-containing corona. This hypothesis, however, requires further investigation for validation. In addition, solution of lower ionic strength (1 mM NaCl) only led to a decrease in hydrodynamic diameter, but no second volume phase transition (exemplarily shown in ESI, Fig. S10(b)†).

Conclusions

To conclude, PVCL-based temperature-responsive microgels with incorporated ionic liquid moieties carrying different counterions were synthesized by two methods: (a) direct copolymerization (pre-functionalization) and (b) post-functionalization. While microgels with all selected anions can be accessed *via* the post-functionalization pathway, only $[MeS]^-$, and $[BF_4]^-$ bearing microgels were obtained in a controlled way from pre-functionalization of the $VIM^+C_nH_{2n+1}[A]^-$ monomers. Depending on the alkyl chain length (n = 1, 12, 16), counterion nature, as well as the applied synthesis route, differences in the volume phase transition temperature, hydrodynamic diameter in swollen and collapsed state, as well as in the electrophoretic mobility were determined. Changes in the microgel solution behavior can be explained by the increase in chaotropic nature given by the Hofmeister series. All obtained microgels showed a LCST-like behavior in ultrapure H_2O. Moreover, the electrophoretic mobility in the swollen state was found to be strongly dependent on the alkyl chain length and counterion in case of post-functionalization. Further investigations on the location of the counterions either being in the outer sphere of the microgels or even penetrating the microgel network could improve the understanding of the observed effects. A promising change in microgel morphology was found for poly(VCL-*co*-$VIM^+C_{12}H_{25}[BF_4]^-$) microgels obtained *via* pre-functionalization, which also resulted in a dual phase transition in aqueous solution of increased ionic strength (I = 10 mM). Future studies will focus on the control of the anisotropic morphology of these microgels with regard to comonomer content and cross-linking density. In addition, alkyl chain lengths of $1 < n < 12$ are of interest for further studies supposing a controlled microgel formation. Differences in the cation–anion interaction strength have been reported for non-polymerizable vinylimidazolium ionic liquids bearing short alkyl chains.[44]

The obtained microgels are interesting colloidal carriers for the uptake of functional molecules with either opposite charge or hydrophobic nature. Moreover, the strong interactions between cationic microgels and anions can be applied in the development of materials with self-healing properties.[45]

Author contributions

T. B.: coordination and execution of the research activity and analysis of the data. Preparation of the published work, specifically writing and correcting the initial draft. M. L.-B.: performing experiments on the microgels functionalized with $VIM^+C_1H_3[A]^-$ comonomers supported and supervised by T. B. A. P.: acquisition of the financial support for the project leading to this publication and revision of the initial draft.

Conflicts of interest

The authors declare no competing financial interest.

Acknowledgements

We thank the German Research Foundation (DFG) Collaborative Research Centre 985 "Functional Microgels and Microgel Systems" for financial support. Further, we express our gratitude for the electron microscopy images recorded by Stefan Hauk, and DSC measurements performed by Claudia Pörschke. T. B. further thanks Kristína Rabatinova for her support as student helper.

References

1 F. A. Plamper and W. Richtering, *Acc. Chem. Res.*, 2017, **50**, 131–140.
2 M. Karg, A. Pich, T. Hellweg, T. Hoare, L. A. Lyon, J. J. Crassous, D. Suzuki, R. A. Gumerov, S. Schneider, I. I. Potemkin and W. Richtering, *Langmuir*, 2019, **35**, 6231–6255.
3 M. Nöth, L. Hussmann, T. Belthle, I. El-Awaad, M. D. Davari, F. Jakob, A. Pich and U. Schwaneberg, *Biomacromolecules*, 2020, **21**, 5128–5138.
4 C. Hu, W. Xu, C. M. Conrads, J. Wu and A. Pich, *J. Colloid Interface Sci.*, 2020, **582**, 1075–1084.
5 T. Hoare and R. Pelton, *Macromolecules*, 2004, **37**, 2544–2550.
6 M. Annegarn, M. Dirksen and T. Hellweg, *Polymer*, 2021, **13**, 1–17.
7 L. Hussmann, T. Belthle, D. E. Demco, R. Fechete and A. Pich, *Soft Matter*, 2021, **17**, 8678–8692.
8 W. Xu, A. A. Rudov, R. Schroeder, I. V. Portnov, W. Richtering, I. I. Potemkin and A. Pich, *Biomacromolecules*, 2019, **20**, 1578–1591.
9 D. Kehren, C. M. Lopez, S. Theiler, H. Keul, M. Möller and A. Pich, *Polymer*, 2019, **172**, 283–293.
10 L. Etchenausia, E. Villar-Alvarez, J. Forcada, M. Save and P. Taboada, *Mater. Sci. Eng., C*, 2019, **104**, 109871.
11 X. Xu, G. R. Shan and P. Pan, *J. Appl. Polym. Sci.*, 2016, **133**, 44132.
12 M. Constantin, S. Bucatariu, P. Ascenzi, B. C. Simionescu and G. Fundueanu, *React. Funct. Polym.*, 2014, **84**, 1–9.
13 T. Belthle and A. Pich, *Mol. Syst. Des. Eng.*, 2022, **7**, 1207–1227.

14 R. A. Gumerov, E. Gau, W. Xu, A. Melle, S. A. Filippov, A. S. Sorokina, N. A. Wolter, A. Pich and I. I. Potemkin, *J. Colloid Interface Sci.*, 2020, **564**, 344–356.
15 T. Watanabe, Y. Nishizawa, H. Minato, C. Song, K. Murata and D. Suzuki, *Angew. Chem., Int. Ed.*, 2020, **59**, 8849–8853.
16 F. Grabowski, V. S. Petrovskii, F. Fink, D. E. Demco, S. Herres-Pawlis, I. I. Potemkin and A. Pich, *Adv. Sci.*, 2022, **9**, 2204853.
17 S. Ravula, S. N. Baker, G. Kamath and G. A. Baker, *Nanoscale*, 2015, **7**, 4338–4353.
18 H. Hu, B. Wang, B. Chen, X. Deng and G. Gao, *Prog. Polym. Sci.*, 2022, **134**, 101607.
19 E. Karjalainen, V. Aseyev and H. Tenhu, *Macromolecules*, 2014, **47**, 7581–7587.
20 E. Karjalainen, V. Aseyev and H. Tenhu, *Macromolecules*, 2014, **47**, 2103–2111.
21 S. Jana, Y. Biswas, M. Anas, A. Saha and T. K. Mandal, *Langmuir*, 2018, **34**, 12653–12663.
22 M. T. Rahman, Z. Barikbin, A. Z. Badruddoza, P. S. Doyle and S. A. Khan, *Langmuir*, 2013, **29**, 9535–9543.
23 S. Chen, A. Chang, X. Lin, Z. Zhai, F. Lu, S. Zhou, H. Guo and W. Wu, *Polym. Chem.*, 2018, **9**, 1439–1447.
24 X. Qu, Y. Zhao, Z. Chen, S. Wang, Y. Ren, Q. Wang, J. Shao, W. Wang and X. Dong, *Research*, 2021, **2021**, 9845482.
25 A. Schindl, M. L. Hagen, S. Muzammal, H. A. D. Gunasekera and A. K. Croft, *Front. Chem.*, 2019, **7**, 347.
26 H. Fang, J. Wang, L. Li, L. Xu, Y. Wu, Y. Wang, X. Fei, J. Tian and Y. Li, *Chem. Eng. J.*, 2019, **365**, 153–164.
27 Z. Fallah, E. N. Zare, M. A. Khan, S. Iftekhar, M. Ghomi, E. Sharifi, M. Tajbakhsh, N. Nikfarjam, P. Makvandi, E. Lichtfouse, M. Sillanpaa and R. S. Varma, *Adv. Colloid Interface Sci.*, 2021, **294**, 102454.
28 T. Belthle, D. E. Demco and A. Pich, *Macromolecules*, 2022, **55**, 844–861.
29 C. L. Tarver, Q. Yuan and M. L. Pusey, *Crystals*, 2021, **11**, 1166.
30 M. A. R. Martins, C. M. S. S. Neves, K. A. Kurnia, A. Luís, L. M. N. B. F. Santos, M. G. Freire, S. P. Pinho and J. A. P. Coutinho, *Fluid Phase Equilib.*, 2014, **375**, 161–167.
31 N. Hazrati, M. Abdouss, A. A. Miran Beigi, A. A. Pasban and M. Rezaei, *J. Chem. Eng. Data*, 2017, **62**, 3084–3094.
32 R. W. Berg, *Monatsh. Chem.*, 2007, **138**, 1045–1075.
33 J. Meyer-Kirschner, M. Kather, A. Pich, D. Engel, W. Marquardt, J. Viell and A. Mitsos, *Appl. Spectrosc.*, 2016, **70**, 416–426.
34 F. A. L. Janssen, M. Kather, L. C. Kröger, A. Mhamdi, K. Leonhard, A. Pich and A. Mitsos, *Ind. Eng. Chem. Res.*, 2017, **56**, 14545–14556.
35 H. J. M. Wolff, M. Kather, H. Breisig, W. Richtering, A. Pich and M. Wessling, *ACS Appl. Mater. Interfaces*, 2018, **10**, 24799–24806.
36 T. Hoare and R. Pelton, *Curr. Opin. Colloid Interface Sci.*, 2008, **13**, 413–428.
37 J. Gao and B. J. Frisken, *Langmuir*, 2005, **21**, 545–551.
38 J. S. Hyatt, C. Do, X. Hu, H. S. Choi, J. W. Kim, L. A. Lyon and A. Fernandez-Nieves, *Phys. Rev. E: Stat., Nonlinear, Soft Matter Phys.*, 2015, **92**, 030302.
39 J. S. Hyatt, A. M. Douglas, C. Stanley, C. Do, T. H. Barker and A. Fernandez-Nieves, *Phys. Rev. E*, 2017, **95**, 012608.
40 R. Marcilla, M. Sanchez-Paniagua, B. Lopez-Ruiz, E. Lopez-Cabarcos, E. Ochoteco, H. Grande and D. Mecerreyes, *J. Polym. Sci., Part A: Polym. Chem.*, 2006, **44**, 3958–3965.
41 X. Zhou, Y. Zhou, J. Nie, Z. Ji, J. Xu, X. Zhang and B. Du, *ACS Appl. Mater. Interfaces*, 2014, **6**, 4498–4513.
42 A. A. Polotsky, F. A. Plamper and O. V. Borisov, *Macromolecules*, 2013, **46**, 8702–8709.
43 G. Marcelo, L. R. P. Areias, M. T. Viciosa, J. M. G. Martinho and J. P. S. Farinha, *Polymer*, 2017, **116**, 261–267.
44 J. Ranke, A. Othman, P. Fan and A. Muller, *Int. J. Mol. Sci.*, 2009, **10**, 1271–1289.
45 J. Cui, F.-M. Nie, J.-X. Yang, L. Pan, Z. Ma and Y.-S. Li, *J. Mater. Chem. A*, 2017, **5**, 25220–25229.